Subarctic physicochemical weathering of serpentinized peridotite

O.I. Ulven[1], H. Austrheim[1], A. Beinlich[1,2], J. Hövelmann[1,3], and B. Jamtveit[1]

[1]Physics of Geological processes (PGP), University of Oslo, 0316 Oslo, Norway

[2]Mineral Deposit Research Unit (MDRU), Department of Earth, Ocean and Atmospheric Sciences, The University of British Columbia, Vancouver, BC V6T 1Z4, Canada

[3] Institut für Mineralogie, University of Münster, D-48149 Münster

Abstract

The reduced availability of liquid water and the prevailing low temperature limits the contribution of chemical weathering to saprolite and soil formation in arctic and subarctic climate zones. In contrast, mechanically driven rock disintegration resulting from ice growth within fractures represents an effective weathering mechanism in cold climate zones, on small scales particularly during diurnal freeze and thaw cycles common in spring and fall months, and on larger scales particularly during sustained freezing well below zero in winter months. However, low temperature fluid rock interaction is an important preconditioning step for subsequent ice cracking as small scale mineral dissolution reactions not only generate porosity and hence fluid pathways but also weaken the rock thus facilitating ice driven fracture propagation at sub critical stress intensity factors. Here we present new insight into processes of subarctic saprolite formation on ultramafic bedrock by combining textural and mineralogical observations on natural samples with a discrete element model describing the mechanical behaviour and fracture formation in a solid when subject to pressure from a growing ice crystal inside an initial fracture. Furthermore, the mechanical model is coupled with a reaction-diffusion model that describes rock weakening by brucite dissolution. The choice of including brucite dissolution into the model is based on our observations of weathered variably serpentinized harzburgite and dunite samples from the Feragen Ultramafic Body (FUB), SE-Norway. The natural samples display well-defined cm to dm thick weathering rinds with elevated porosity relative to unweathered parts of the sample, which is attributed to the dissolution of brucite (Mg_0.92 Fe_0.08 (OH)_2) during weathering. In contrast, olivine (Fo_92-93) and serpentine (FORMULA) are chemically almost inert under the prevailing conditions but control the shape and propagation direction of the formed fractures. This modeling strategy reproduces observations of both cm scale meandering fractures that penetrate into the fresh part of the rock, and dm scale fractures that deform the surface and initiate breakup of large domains. Disintegration during weathering increases a rock's reactive surface area and hence its susceptibility to mass transport of dissolved and particulate matter in the weathering fluid and the overall CO_2 uptake potential due to formation of carbonate coatings on gravel surfaces. Additionally, formation of secondary carbonate minerals in the pore space and fractures may exert an additional force that drives the disintegration of weathering surfaces. Therefore, our observations have implications for

element cycling between the continents and oceans and uptake of atmospheric CO_2 both in nature and mine tailings.

Keywords:

Peridotite

Sub-arctic weathering

Brucite dissolution

Carbonation

Frost fracturing

1. Introduction

Chemical and physical processes within the critical zone driven by the interaction between the atmosphere and the Earth's surface control the amount and rate of mass transport between geochemical reservoirs on short and intermediate time-scales (Brantley et al., Elements 2007). An important example is the uptake of atmospheric CO_2 due to weathering of Ca- and Mg-silicate minerals and subsequent carbonate precipitation. These minerals are concentrated in mafic (e.g., basalt, gabbro) and ultramafic (e.g., dunite, peridotite) rocks. Element uptake and release during weathering is to a large extent controlled by the different dissolution rates of minerals during interaction with rainwater. Generally, the dissolution rates of the most abundant mafic and ultramafic minerals decrease in the order brucite>>olivine>pyroxene>serpentine, making dunite and peridotite viable targets for natural mineral carbonation studies in addition to basalt. Numerous experimental (Hövelmann et al., 2011, 2012; van Noort et al., 2013; Andreani et al., 2009; Giammar et al., 2005; King et al., 2010; Daval et al., 2011) and natural analog studies (Beinlich and Austrheim, 2012; Beinlich et al., 2010; Beinlich et al., 2012; Kelemen and Matter, 2008; Oskierski et al., 2013 a and b, Boschi et al., 2009; Hansen and Dipple, 2005) have investigated the potential of ultramafic rocks as a feedstock for carbonate formation to mitigate anthropogenic CO_2. Other environmental aspects associated with ultramafic rock weathering are the release of asbestos and fluid mobile toxic Ni- and Cr-bearing compounds into agricultural land and drinking water (Bales et al., 1984; Dublet et al., 2012; Garnier et al., 2013; Holmes et al., 2012; Oze et al., 2007). Tropical peridotite weathering has formed economically significant Ni-laterite deposits (Golightly and Arancibia, 1979; Wells et al., 2009). Ultramafic rock weathering usually results in the formation of clay minerals (smectite, montmorillonite) and occasionally minerals of the hydrotalcite group (e.g. pyroaurite) also known as anionic clays (Miyata, 1983), which have found extensive use as catalysts and in environmental chemistry to retain hazardous ions (Koch, 1998; Rozov et al., 2010). Due to the interest in soil formation and their toxicity, studies of ultramafic rock weathering are focused in tropical and temperate climate zones where laterite formation often results in depletion in Ca, Mg and Si and enrichment in Fe and potentially toxic metals such as Co, Cr and Ni (Oze et al., 2007; Schwertmann and Latham, 1986). However, besides recent investigations of the natural

carbon uptake potential of ultramafic mine wastes in Canada (Pronost et al., 2011; Wilson et al., 2011; Wilson et al., 2009) little is known about ultramafic rock weathering in the arctic and subarctic climate zones.

The Feragen ultramafic body is located in the subarctic climate zone, where the temperature in autumn and spring fluctuates around 0°C, giving rise to fast freeze-thaw cycling. In winter, stable temperatures well below zero are common. This suggests that frost driven weathering could be an important process in such areas. The reason for frost cracking has been debated (see e.g. Walder and Hallet, 1985), with the current view being that ice segregation is the main driving force for the cracking. The 9% volumetric expansion of water during freezing is regarded an effective reason for cracking only during rapid freezing in diurnal time periods within a few centimetres of the surface of nearly water saturated rocks (Matsuoka and Murton, 2008; Girard et al., 2013). Freezing damage on the time scales of a winter season are generally caused by ice segregation, in which unfrozen water, either located in small pores where the freezing point is reduced due to curvature effects, or in a rock volume where the temperature is above the freezing point, migrates to freezing centers due to cryosuction (Walder and Hallet, 1985; Rempel et al., 2004). This can cause much stronger damage than the repeated freeze-thaw cycling (Girard et al., 2013), and typically produces fracturing on larger scales, potentially reaching several meters into the bedrock (Matsuoka and Murton, 2008). The process could also be further accelerated by refreezing of snowmelt water penetrating into fractures during thawing (Matsuoka, 2008). A rock's susceptibility to frost weathering depends on the porosity and strength of the rock. Lautridou and Ozouf (1982) concluded that a rock with porosity less than 6% was not frost sensitive, while Matsuoka and Murton (2008) stated that low porosity rocks were not susceptible to frost when intact, but could disintegrate along pre-existing joints. On the other hand, high-porosity rocks are known to be sensitive to frost (e.g. Matsuoka and Murton, 2008). Frost weathering is commonly studied in rocks with homogenous porosity, but the coupled process of frost weathering and chemical processes that weakens the rock and induce porosity in initially tight rocks seems to have received less attention.

Here we present new insight into the chemical, physical and mineralogical processes taking place during saprolite formation at the Feragen Ultramafic Body (FUB) in SE-Norway, and present a model for the coupling between frost damage and chemical weathering. The

Weichselian glaciation constrains the age of the formed saprolite to less than 10 ka and its small thickness yields constraints on element mobility, vein-growth, carbonation and mechanical fragmentation at the atmosphere-rock interface. Cold climate ultramafic rock weathering studies may further our understanding how to design mine waste piles to optimize their carbon uptake potential and minimize the risk of toxic waste water generation.

In an accompanyig paper (Austrheim et al., in prep), we focus on the mineralogical and geochemical changes that occur during deeper weathering in the tectonic (fault-) zones of the Feragen Complex.

2. Geological and climatic setting of the FUB

The FUB is situated in east central Norway (62˚32.9'N 11˚48.4'E) at an altitude between 700 and 900 m a.s.l. between the town of Røros and the border with Sweden (Fig. 1). The area is among the coldest regions in Europe with monthly mean temperatures ranging between -25 and +8 °C (see http://eklima.met.no). The area is barren with prominent rock exposure covered by a thin (<0.8 m) layer of saprolite alternating with peaty areas (Fig. 2a). As most parts of Scandinavia, the FUB was completely glaciated during the Weichselian which constrains the maximum age for the observed surface weathering and saprolite formation to <10 ka. The FUB is one of several ultramafic bodies that are aligned over a distance of >200 km across the Norwegian-Swedish border. It has been regarded as an alpine peridotite in gneissic Cambro-Silurian sequences (Moore and Hultin, 1980). The FUB comprises partly serpentinized dunite and peridotite together with harzburgite and chromitite layers. The degree of serpentinization varies between almost complete in the outer parts of the FUB and partial in the central part. The northern contact with the surrounding country rocks is covered by a Devonian serpentine conglomerate indicating that the FUB was exposed to surface weathering already in the Paleozoic. Moore and Hultin (1980) report on small occurrences of Mg-carbonates (magnesite, nesquehonite) along fractures and cleavage surfaces in serpentine and chlorite. During the 19th century, the FUB was extensively mined for chromite until mining ceased at around 1927 and has not been resumed ever since.

3. Analytical methods

3.1 Raman method description

A confocal Raman spectrometer (Horiba Jobin Yvon XploRA) operating with the 638 nm line of aNd:YAG laser was used for spatially resolved identification of mineral phases within the serpentine and carbonate veins of weathered and unweathered parts of the samples. Single spectra were takenwith a 500 μm hole, 100 μm slit and 1200 grooves per millimeter grating using an acquisition time of4 x 45 s. Corrections for system drift were done using the 520.7 nm Raman band of a silicon standard taken at the beginning and the end of each measuring session. Raman maps across the weatheringinterface were obtained using a step size of 1 x 1 μm and an acquisition time of 2 x 60 s. At eachpoint of the map a Raman spectrum was taken in the 100−800 cm−1 region. The Labspec software was used for peak fitting and for producing intensity maps of selected Raman bands.

3.2 Backscattered electron (BSE) imaging

Back-scattered (BSE) images of thin sections were collected both with a JEOL JSM 640 LV scanning electron microscope and a SX100 electron microprobe (Institute of Geosciences, University of Oslo).

4. Observations

The FUB is variably serpentinized, and we consider serpentine as a primary phase with respect to minerals formed during surface weathering. Besides serpentine, the pre-weathering mineralogy consists of brucite $(Mg_{0,92}Fe_{0,08})(OH)_2$, olivine (Fo91-93), orthopyroxene, clinopyroxene, Cr-spinel and awaruite.

4.1. Field observations

The ultramafic rocks of the FUB display fracturing on scales ranging from km to mm and with different intensities. Large-scale, km-sized fault and deformation zones are restricted to the outer part of the FUB close to the contact with the surrounding country rocks. These parts were also subject of intense serpentinization and carbonation. The partly serpentinized central part of the FUB exhibits a hierarchical-looking (cf. Iyer et al., 2008) fracture pattern with dominantly four sided m^2-sized domains truncated by fractures reaching up to several 10's of m in length. Parallel fractures are often observed, and commonly at least three different sets of

dominating fracture directions are observed (Fig. 2a). Intersection angles are controlled by the angle between the dominating directions, producing both ~90° angles and angles that deviate significantly from 90°. The observed fractures usually continue straight through intersections, instead of terminating in T-junctions. Drill cores from the bottom of such fractures show that the fractures correlate with thick preexisting serpentine veins that seem to control the fracture patterns formed.

Centimeter sized fractures are associated with surface spallation resulting in the formation of a surface cover composed of cm-sized, angular and often flaky rock chips (saprolite) around and on the surfaces of the exposed bedrock. The saprolite thickness varies between a few cm and 0.8 m and may be thicker in small topographic depressions along tectonic zones. On rock surfaces, the meter-sized hierarchical-looking fractures have developed mm to cm wide reaction zones that form small (<1 cm) and brittle outstanding edges around otherwise flat rectangular domains (Fig. 2b). Locally, weathering and rock spallation flattens these edges to produce gravel that is deposited inside the open fractures or on the rock surface (Fig. 2c). On topographic heights, most gravel is transported away, and fractures may form cm to dm wide and several dm deep crevasses often partly filled with gravel (Fig. 2d). Weathering and spallation tends to smooth rock edges produced by the breaking of larger rock pieces thus forming ball shaped humps of bedrock resembling onion skin weathering (Fig 2d). In this process, larger blocks are broken loose (Fig. 2e), leaving significant amounts of gravel in the fracture.

We also notice that the dunites are markedly more weathered than the pyroxene containing peridotites and are covered by a thicker layer of debris.

4.2. **Textural and mineralogical observations**

Polished slabs through hand specimen samples of dunite reveal that weathering results in the formation of an inner bluish and an outer yellowish alteration zone (Fig 3a). The blue inner reaction zone has sharp interfaces to the pristine serpentinized dunite and the yellow outer zone, the zones are typically <2 cm thick. Interfaces are generally wavy and form wedge shaped indentations toward the unweathered inner part of the sample. Fractures filled with carbonate regularly extend from the wedgeshaped indentation into the interior of the sample

(Fig. 3b). Such fractures may take on a meandering form as they continue deeper into the pristine part of the sample (Fig. 3c) where their path may be controlled by the orientation of grain boundaries or preexisting serpentine veins. Locally, small (<0.5 cm in thickness), worm-like, outstanding surface perturbations can be observed on hand speciments (Fig. 3d). These are not related to larger fractures, and drill cores indicate that these pertubations correspond to thin serpentine veins which reach the surface at an oblique angle. Fractures can often be followed from the wedgeshaped indentations outwards where they connect to such ridges on the surface of the rock. In areas subject to fresh rainwater, the outer cm OR CMS? of surface connected fractures is open, while in more sheltered areas the fractures are often filled with carbonate.

The transition from the weathered to the unweathered zone is sharp on micrometer scale, with sharp wedges penetrating into the pristine part (Fig. 4a). Optically, the weathering front is characterized by a pronounced color change in the serpentine veins from darker brownish in the weathered part to brighter greyish in the unweathered part (Fig. 4b). Relict olivine grains appear unaffected by the weathering process and are approximately equally abundant in the weathered and unweathered parts. The sharp wedges often correlate with open fractures in the weathered part.

Scanning electron microscope observations reveal an abundance of thin meandering fractures (Fig. 5a) running mainly along preexisting serpentine veins, and most often avoiding relict olivine grains. The fractures are usually open in the weathered part of the rock, with a gradual transition to being filled by a porous hydrocarbonate in the unweathered area (Fig. 5b). A thin open fracture is often seen along the carbonate, sometimes also cutting through it. This indicate a late deformation of the rock postdating carbonate growth. Fractures penetrating into the unweathered part are typically surrounded by 100-200 μm wide zones of high porosity.

4.3 Brucite dissolution, porosity generation and carbonate precipitation

Extensively serpentinized samples, and in particular the dunite samples, display a typical mesh texture composed of serpentine veins surrounding relict olivine fragments.

Brucite is abundant in serpentinized dunite samples both as larger grains within mesh cells and in veins, typically intergrown with serpentine on a submicroscopic scale.

The transition from the unweathered material to the dark weathered material (Fig. 6a) correlates with a sharp increase in porosity (Fig. 6b), indicating that the weathering process is related to porosity formation. Elemental distribution maps of the same front shows a significant reduction in the amount of magnesium in the weathered zone (Fig. 6c), whereas the amount of silica remains unchanged (Fig. 6d). This is consistent with preferential dissolution of brucite in the weathering process.

A detailed Raman mapping of the weathering front reveals that the brucite is dissolved, in a process that is essentially sharp on micron scale (Fig. 7). In the weathered zone, brucite is replaced by pyroaurite, whereas the serpentine is virtually unchanged.

Weathering of the FUB involves precipitation of secondary hydrotalcite and hydrocarbonate phases. Pyroaurite (hydrotalcite) is commonly present in the weathering zone. Secondary hydrous Mg-carbonate phases are abundant weathering products, and are present as cement between fragmented ultramafic material and as vein forming phases. Dypingite has been detected as vein mineral and surface coating on ultramafic spree based on its appearance on secondary electron images, XRD analyses revealed the presence of additional artinite. Nesquehonite was reported by Beinlich and Austrheim (2012) from open pits in the FUB

5 Numerical modeling

5.1 Model description

A two dimensional coupled model of reaction-diffusion and deformation previously used to study volume increasing reactions (Ulven et al., 2014) was modified to include effects of ice wedge growth and mechanical weakening due to dissolution of brucite. The mechanical model is a discrete element model (DEM) (Cundall and Strack, 1979), in which the modeled domain is filled with a collection of particles joined by solid beams withstanding both tensile and shear stresses. A fracture is represented by the irreversible removal of a beam that is subject to too high stresses. The fracture criteria are based on a Coulomb critical stress criterion and a maximum tensile stress criterion (Pollard and Fletcher, 2005).

The reaction-diffusion model is based on the transport of a mobile reactant W, in this case

water, being transported into the rock by effective diffusion in bulk material and instantaneous transport in fractures. The mobile reactant transforms an initial solid A, in this case unweathered rock, into the final solid B, a weathered rock (see Ulven et al. (2014) for details). The effect of the chemical reaction is to reduce both the tensile strength and the compressive strength of the weathered rock by an order of magnitude as compared to the unweathered rock. The effect of increased porosity on fluid transport is ignored, since reasonably sharp reaction fronts can be reproduced without considering porosity changes by choosing appropriate parameters, and our main focus is the fracturing behaviour. Inert olivine grains were included in the domain in some simulations, these did not take part in the chemical reaction, but were mechanically an order of magnitude stronger than the unweathered serpentine.

The numerical model was run on a square domain with the upper boundary kept mechanically free, and the lower boundary fixed in the vertical direction. The sides were either kept free or completely fixed, to see the effect of confinement. Only the upper surface was available for fluid infiltration. Material properties for serpentine and olivine were distributed according to a mesh texture taken from sample RØR02-08 for a mm–cm scale study, and homogenous properties were used for a cm–dm scale study.

An initially weathered layer equal to 3% of the domain height was defined on top of the domain (Fig. 8), and a vertical fracture of length 7% of the domain height was initiated. The ice wedge was introduced by defining the upper 5% of the preformed fracture to contain the ice. Since fractures penetrating into the unweathered domain usually are filled by hydrocarbonates (Fig. 5b), ice growth will be hindered there. It is thus assumed that the ice wedge is limited to mainly the weathered zone and a short distance into the unweathered material, where the fractures are usually open or semi-open. Since fractures driven into the unweathered domain are obviously advancing faster than the weathering front – otherwise, no fractures would be able to penetrate into the unweathered domain – it is assumed that the ice wedge has approximately constant length for the time simulated. The wedge was assumed to exert the same pressure on all surfaces, and the pressure was initially set to zero. The pressure was then gradually increased until either an assumed maximum crystallization pressure was reached, or the rock started breaking. If the rock started breaking, the pressure was gradually reduced, until the fracture stopped growing. The reasoning behind this approach is that we

assume that water availability will limit the ice growth. Then, the reaction-diffusion model was run one time step, simulating weathering of a thawed rock in the summer season, before the ice growth process was repeated. This stepwise procedure, reproducing seasonal freeze-thaw, was run until a satisfactory fracture had been formed.

Assuming abundant supply of liquid water, the maximum crystallization pressure is approximately 1.1 MPa per degree below freezing (Dash et al., 1995). We have assumed a maximum pressure in the range 0.5–10 MPa in the simulations. Several combinations of maximum pressures and degree of confinement were tested.

The following mechanical properties were used: Young's modulus E = 100 GPa, Poisson ratio n = 0.25, compressive strength of serpentine C_u = 0.33 GPa, tensile strength of serpentine T_u = 20 MPa, friction angle m = 0.9

5.2 Model results

Low ice pressures and little confinement generally resulted in formation of meandering fractures (Fig. 9a). The growing ice wedge is exerting a tensile stress at the tip of the fracture within which it is contained. This makes the fracture penetrate gradually into the rock, in a feedback process where ice breaks the rock, thus increasing the rate of water transport into the rock, and localized brucite dissolution along the fracture weakens the rock. This localization, in combination with the strong olivine grains, gives the fracture a meandering shape. For the lowest pressures, there was no significant surface deformation, but the fracture only penetrated a short distance before stopping. The pattern in Fig. 9a is a result of using a maximum pressure of 4 MPa, with mechanically free sides. Under such conditions, the fracture was able to penetrate through the entire domain, although large grains could block the fracture's path, and hinder further fracture growth for a significant time. This could be a purely two dimensional effect. Increasing confinement reduced the amount of fracture growth.

High ice pressures and high confinement formed large aperture fractures that did not penetrate deep into the rock (Fig. 9b). Instead, the crystallization pressure was sufficient to initiate a

dense network of shear fractures due to compression in the weathered material around the ice wedge, and the material was pushed outwards and upwards by the growing ice, forming ridges along the fracture.

6. Discussion

Textural observations in the pristine and weathered parts of the investigated samples indicate that the fastest dissolving primary phase is brucite in agreement with experimental data (Pokrovsky and Schott, 2004; Zhao et al., 2010; Hövelmann et al., 2012) and field observations (Beinlich and Austrheim, 2012; Hostetler et al., 1966). Partial to complete dissolution of brucite during weathering results in the formation of porous mesh cells and veins in the blue and yellow weathering zones. This increases fluid transport rates, weakens the rock by removing the brucite «glue» inside the serpentine mesh, and finally makes the rock susceptible to frost cracking. The approximately constant modal abundance of olivine in pristine and weathered sample parts suggests that olivine behaves almost inert during weathering of the FUB.

The brucite content of non-weathered samples varies throughout the FUB. Completely serpentinized dunites contain the highest amounts of brucite, and are commonly seen to be completely fragmented. Partly serpentinized peridotite, which contains less or even no brucite, due to a significant initial pyroxene content, can be almost unweathered. Next to it, heavily weathered dunite-lenses with comparable degree of serpentinization can often be found. The FUB is crosscut by a dense network of thick serpentine veins in some areas, and these provide an important control on the weathering rate and pattern developed in such areas.

The primary weathering front between the unweathered part and the blue zone where all brucite is dissolved, is always sharp. This is a common effect of porosity changes during weathering (e.g. Navarre-Sitchler et al., 2011), due to higher water content in the porous weathered rock. As the water content increases, the brucite dissolution rate also increases, and the result is that brucite will locally be either almost completely dissolved or still fully intact. Local differences in fluid transport rates makes the brucite dissolution faster in some areas, explaining the wedge shaped indentations observed toward the unweathered part (Fig. 3, 4).

As brucite is dissolved, the water pH rises. The dissolution rate of brucite generally decreases with increasing pH, and becomes virtually zero for pH>10 (Pokrovsky and Schott, 2004; Hövelmann et al., 2012) Along surfaces that are subject to moderate pH surface waters, the weathering zone is generally depleted in both brucite and hydrocarbonates (upper weathered zone of the hand sample shown in Fig. 3b). The dissolved hydrocarbonates are either reprecipitated elsewhere or transported away by the local runoff (Beinlich et al., 2014). Brucite dissolution is also present where the surface is more protected from fresh surface waters (lower weathered zone of the hand sample shown in Fig. 3b), but in this case, hydrocarbonates can also be present. In fractures that penetrate beyond the main weathering front (meandering fracture in Fig. 3c), carbonates are often seen to precipitate, while brucite is dissolved (Fig. 5a). These observations indicate that higher pH than typical rain water is required to form hydrocarbonates, but that hydrocarbonates precipitate at a pH where brucite is still dissolved. When high pH waters reach open air in areas protected from fresh rain water, as in the mines studied by Beinlich and Austrheim (2012), significant amounts of carbonates precipitate using magnesium cations from the dissolved brucite and CO2 from the air.

The secondary weathering front, between the blue and yellow weathered material, does not seem to change the porosity significantly.

The mesh textures observed in the weathering of the FUB resembles the textures presented by van Noort et al. (2013). They performed laboratory experiments on dissolution of olivine in partly serpentinized dunites, and found that the serpentine veins accelerated the process by providing faster transport of the solvent. They also reported lower Mg/Si ratios in serpentine veins close to the sample surface than deeper into the sample. Although they don't state explicitly that this is due to dissolved brucite in the serpentine veins in their experiments, it seems reasonable to assume that brucite dissolution is controlling that process, as well. This indicates that the presence of brucite-containing serpentine veins might be important for accelerating carbonation of olivine. It also suggests that partially serpentinized dunites are better targets for carbonation than pure olivine, even though the dissolution rate of serpentine itself is lower than for pure olivine.

Wedge shaped indentations into the unweathered material (Fig. 3) could indicate a volume increasing process in the weathered material. Volume expansion often forms fractures penetrating into the unreacted domain (Ulven et el., 2014), and localized reaction along such fractures take the shape of a wedge (e.g. Røyne et al., 2008). However, the presence of open fractures cutting through the weathered material does not indicate any volume expansion. Growth of ice in these open fractures is assumed to be the driving force for this wedging and fracturing, as is indicated by the results of section 4.4.

It seems reasonable to assume that the porous weathered rock at the FUB is sensitive to ice driven fracturing, whereas the unweathered rock is probably insensitive to frost cracking, apart from potential reopening of the weakest serpentine veins. The fracture growth rates are probably low, since little water is available for migration to freezing centers and water migration is slow in tight rocks. However, large growth rates reported for porous rock in other literature (e.g. Walder and Hallet, 1985) illustrate that it is reasonable to assume that the observed fracture patterns could have been formed by frost cracking during the time since the Weichselian glaciation.

The model used to study fracture formation in section 5 indicates that when the maximum ice crystallization pressure is sufficiently low, which would occur in cases where the water supply is limited, fractures will not grow without rock weakening due to brucite dissolution. This results in a meandering fracture in the unweathered zone (Fig. 9a), where dissolution and fracture growth is coeval. This type of process also fits the observation in Fig. 5b, where an open fracture is following and cutting the hydrocarbonate filling. We infer that the carbonate has originally filled the entire fracture, and ice growth in the outer part of the fracture has subsequently widened the fracture aperture. Higher crystallization pressures give a significant surface deformation, with formation of fractured ridges and a large aperture fracture in the weathered material (Fig. 9b). The high fracture density in the ridges produced by the model is consistent with the fact that the ridges observed in the field (Fig. 2b) were too fragile to be sampled. The large aperture fracture that does not penetrate very deep also fits field observations, and leads us to argue that the water availability is higher in the major serpentine veins present in field areas like the one in Fig. 2a. This could be due to additional pore space along the serpentine vein, although refreezing of snow melt water could also be important.

Since water availability and material strengths, especially of the weathered material, are unknown, and the observed fractures are the result of a complex history of freezing, it is difficult to make any quantitative study of the frost weathering. Our highly simplified model, which ignores details like the initial mechanism of fracture nucleation, water migration, heat transport, ice geometry and nucleation of new ice crystals, is intended to serve as a qualitative study of what different fracture phenomena could occur in different settings. In the model, observed features are satisfactorily reproduced when using pressures that are within the expected range at typical winter temperatures (e.g. Dash et al., 1995) and material strengths within typical values for crystalline rocks (Pollard and Fletcher, 2005). It seems reasonable to assume that an appropriate ice pressure could reproduce the same features for different material strengths as well.

Diurnal freezing cycles, which typically results in the prying away of mineral grains and rock flakes producing rock fragments up to pebble size (Matsuoka and Murton, 2008), might explain the abundance of flaky gravel observed at the FUB (Fig. 2c). This process requires high saturations of water in the pore space (Matsuoka and Murton, 2008), indicating that the fracture intensity will be higher in local topographic depressions, where surface water accumulates (Girard et al., 2013). Thus, a fracture initiated at a surface can serve as a positive feedback, localizing surface water and further frost cracking. This fact, in combination with the numerical results from section 4.4, leads us to suggest the frost weathering mechanisms presented in Fig. 10.

In both suggested mechanisms, it is assumed that an ice wedge is nucleated in a weak zone forming a right angle with the surface. Significant deviations from right angles would rather make the ice pry away a rock flake, and not form a deep penetrating fracture. The first process illustrated in Fig. 10 describes a grain scale fracture growth mechanism. The fracture grows gradually, in a process where the ice drives the fracture a short distance, and subsequent brucite dissolution weakens the rock. At a somewhat larger scale in the second mechanism, fractures follow the weak major serpentine veins. If the crystallization pressure is higher in this setting, it deform the surface, and the deformed, weak surface layer is removed by rapid freezing. This leaves a groove, in which water saturation increases, thus making it more likely to pry away flakes in the bottom of the groove during rapid freezing. Water saturation at the

surface is effectively reduced by surface water draining into the fracture, which also reduces the rate of further fracture formation at the surface. The coupled process of a high crystallization pressure that drives a fracture along the serpentine vein and rapid freezing in a water saturated environment thus forms an open fracture, with aperture on cm to dm scale, that can penetrate deep into the rock.We infer that this process, applied along serpentine veins with different directions, is responsible for the wedging out of separate blocks and formation of large, open fractures as seen in Fig. 2a.

Although the observation of open fractures in the weathered zone in most samples points to ice driven fracturing as the main mechanism of breaking the rock, it has been shown that as water evaporates during drying, the supersaturation with respect to minerals can become high enough to break rocks due to the crystallization pressure (Noiriel et al., 2010). This indicates that carbonate growth during drying periods could participate in the fracturing. However, this is less likely in the meandering fractures, since fracturing driven by internal pressures in sharply curved fractures would almost certainly lead to a more branched network than what is seen. But in heavily serpentinized areas, where the rock is highly fragmented, carbonation could be an important part of the fracturing process. This will be covered in further detail in part two of this paper.

As water freezes, the supersaturation with respect to minerals dissolved in the water can increase, since the minerals are left in the remaining water. This process is similar to mineral supersaturation and subsequent precipitation due to evaporation of water, and is seen in the formation of cryogenic cave carbonates (Zak et al., 2004). Additionally, as water is pulled to a freezing center by cryosuction, water might also migrate from small pores, where mineral precipitation is suppressed due to curvature effects, to larger pores or fractures. When entering larger volumes, the solute can suddenly become supersaturated due to the reduced curvature effect. We propose that increasing supersaturation due to freezing and water migration to larger pores can be an additional mechanism that can drive fracturing due to mineral growth in cold regions, although this has apparently not been investigated previously.

7. Conclusion

The weathering at the FUB critically depends on the initial olivine content of the rock, and its degree of serpeninization. The higher both are, the more brucite is formed, and brucite dissolution is controlling the weathering through porosity generation and rock weakening. A new numerical model indicates that ice drives the observed fracturing at the FUB in a process that is coupled with rock weakening due to brucite dissolution. Supersaturations induced by evaporation of water could also drive precipitation of other minerals, mainly carbonates, that participate in the fracturing, and we propose freezing as another means of achieving the necessary supersaturation.

Carbonate minerals are formed in the process, indicating that serpentinized dunites could be attractive targets for industrial CO_2 sequestration, although the apparent dissolution of carbonates in weathered rock affected by rain water makes the stability of these carbonates somewhat questionable. Additionally, the fast dissolution of brucite increases the available surface area of relict olivine grains significantly, which seems important in achieving extensive olivine carbonation.

Acknowledgements

We thank Dag Dysthe, Anja Røyne and Anders Malthe-Sørenssen for useful discussions and advice during the progress of this work. H.A. acknowledges late Odd Nielsen for the introduction to the Røragen field area.

Figures captions

Fig. 1. Simplified geological map of Feragen Ultramafic body (FUB) modified after Moore and Hultin (1980). The FUB is surrounded by serpentinite along its contact. The sentral part is serpentinized to various degrees.

Fig. 2. Field photos showing weathering phenomena of the Feragen Ultramafite Complex
a) Air-photograph showing barren peridotite with a thin regolith cover. Note regular fracture system. Persons for scale.
b) Detail of weathering rind in peridotite showing that the front locally make a pertubation into the unweathered parts.

c) Spheroidally weathered peridotite. The weathering rind consists of two zones. Platy fragments are formed by spallation from the weathered zones.
d). Block terrain developed by wedged out blocks of peridotite.
e). Detail from 2d. Lifting away one of the blocks (outlined by arrow in Fig. 2d) exposes a white coating of extracellular polymeric substances (EPS).

Fig 3.
a) Cross section through a wedged out block of peridotite from the Feragen Ultramafic complex. The weathering rind consists of two zones – a yellow outer rim and a bluish inner rim. The inner front makes wedged shape pertubations into the partly serpentinized dunite. Note spalling in the yellow zone. Sample Rør 08-08.
b) Cut through peridotite with rigded surface. Note that the weathering continues behind the main weathering front as a thin greyish paths locally with the pattern of a random walk and locally as more straight lines.The veins of deep weathering apparently connect to the ridges. Sample Rør05-10
c) Details from 3b. Note that the blue weathering zone develops a meandering form inside the block.
d) Ridged surface of the sectioned sample shown in 3c. The ridges are ca 0.5 cm high and connect to the straight and meandering veins.

Fig 4
a). Photomicrograph of weathering front seen in Fig 3a. The wedge shaped pertubation end in dark veins penetrating behind the main weathering front. Length of image 0.6cm. Sample Rør08-08.
b). Photomicrograph across weathering front. The colour change following the preexisting serpentine veins suggest that they acted as channels for the weathering fluid. Length of image 0.6 cm. Sample Rør02-08.
Fig. 5.
a). Meandering hydrocarbonate filled veins surrounded by a c. 100 μm thick porosity zone transecting strongly serpentinised dunite. The porosity is formed by dissolution of brucite (br). Sample Rør05-10d.

b).Part of meandering vein transecting serpentinised dunite. The carbonate develops delicate crystals needles suggesting that it grew in an open crack. Note also that the carbonate vein is cut and followed by a thin open fracture suggesting that it grew during a crack-seal mechanism interpreted to result from frezing and thawing cycles. Sample Rør5-10b

Fig. 6. Details of weathering front in strongly serpentinised dunite.
a). Photomicrograph showing weathered serpentinised dunite (upper dark part) and non-weathered serpentinised dunite lower part. The weathering interphase is outlined by the stippled line. Sample Rør 17-11c.
b). BSE image across the same weathering front seen in a. Relict grains of olivine (Ol) occur both in the weathered and nonweathered part. Note that the weathered zone has developed a porosity due to dissolution of brucite. Bright grains are magnetite.
c). X-ray map showing distribution of Mg across the same front. In the nonweaterhed serpentinised part the variation in Mg reflects variation in brucite. At the weathering front the brucite is dissolved, leading to lower Mg content. Black areas are magnetite.
d). X-ray map of Si showing the brucite distribution (green). In the weathered zone the former brucite veins are still visible by their green (low Si) colour in accordance with pyroaurite.

Fig 7.
a) Optical micrograph showing the weathering interface in sample Rør−5−10A. The sharp weathering interface is marked by a notable color change in the serpentine veins. b) Close−up of the area marked with a white rectangle in a). The white rectangle across the weathering interface indicates the area that was chosen for Raman mapping. c) Typical Raman spectra obtained from the serpentine veins in the weathered (red spectrum) and unweathered part (black spectrum). Spectra taken from the unweathered part, display Raman bands of serpentine and brucite (227 and 442 cm−1).
Spectra taken from the weathered part are characterized by the absence of brucite bands and the appearance of the 528 cm−1 band of pyroaurite. d−f) Raman intensity maps for the 442cm−1 band of brucite, the 528 cm−1 band of pyroaurite and the 382 cm−1 band of serpentine, respectively. Note that abrupt changes in the brucite and pyroaurite band

intensities match exactly with the weathering interface. The intensity of the serpentine band is more or less constant over the entire mapping area indicating that serpentine was not affected during weathering.

Fig. 8. Sketch of the geometry used in the simulations. A square domain was defined, and the upper 3% of the domain (dark grey) was set to be weathered at the start of the simulation, while the rest (white) was unweathered. An ice wedge (black, note overexaggerated width) was introduced in the upper 5% of the domain inside a preformed fracture (black+light grey) of length 7% of domain height.

Fig. 9. Result from modeling. a: Meandering fracture on grain scale, width of figure represents approximately 1 cm. Relict olivine grains are shown as green, serpentine is shown in colour scale from brown for brucite containing serpentine to yellow for serpentine where all brucite is dissolved. Open fractures are shown as black. The fracture is driven into the domain by an ice crystal in the upper part of the domain, and the chemical reaction is accelerated along the fracture due to internal fluid transport. The fracture is growing gradually, in a coupled process of brucite dissolution and ice driven fracturing. b: Open fracture on cm–dm scale. The material is assumed to be homogenous, with fixed side boundaries. The fracture penetrates a short distance into the domain, but has a large aperture near the surface, and forms porous and fractured ridges.

Fig. 10. Sketch of fracture mechanism, panels a–e showing a small scale mechanism (mm to cm) and panel f–j illustrating a larger scale (dm) mechanism. Colours are the same for all panels, showing yellow and blue weathered zones, and dark unweathered core. Relict olivine grains are shown in green in panels a–e. a: An ice crystal (turquoise) is nucleated in a large pore or other weak areas in the weathered zone, a fracture (black) is penetrating through the weathered material. b: The rock is thawed, and the water (blue) penetrates into the open fracture. c: The rock freezes, and the now larger ice crystal drives the fracture (gray) a short distance into the unweathered rock in a path that avoids the relict olivine grains. d: Water penetrates into the new fracture in the thawed rock, and starts dissolving brucite along the fracture. The pH is high, and allows precipitation of carbonates (white particles) during drying periods. e: Water freezes in the portion of fracture in the weathered zone. Carbonates

prevent ice nucleation in the fracture penetrating into the unweathered zone, and water is instead pulled to the ice crystal by cryosuction. This drives the fracture further into the unweathered rock. f: A large serpentine vein (green) is dominating the rock, and an ice crystal nucleates where brucite is dissolved along the vein. This drives a fracture into the rock along the vein, in a process similar to what is outlined in a–e. g: Pressure from ice in the fracture has produced porous ridges, and water infiltrates both the fracture and the porous ridges in the thawed rock. h: Rapid freezing in the surface near layer breaks off the ridges, and the large ice crystal drives the main fracture deeper into the rock. i: Spalls are transported away, thus forming a groove above the fracture. Water collects in the bottom of the groove. j: High water saturation in the bottom of the groove gives new fractures localized to the groove bottom upon rapid refreezing, thus forming new spalls. Low water content at the initial surface slows down the surface frost weathering.

References

Bales, R.C., Newkirk, D.D., Hayward, S.B., 1984. Chrysotile asbestos in California surface waters - from upstream rivers through water-treatment. Journal American Water Works Association 76, 66-74.

Beinlich, A., Mavromatis, V., Austrheim, H. and Oelkers, E.H. 2014. Inter-mineral Mg-isotope fractionation during hydrothermal ultramafic rock alteration - Implication for the global Mg-cycle. Earth and Planetary Science Letters, 392, 166-176.

Beinlich, A., Austrheim, H., 2012. In situ sequestration of atmospheric CO_2 at low temperature and surface cracking of serpentinized peridotite in mine shafts. Chem. Geol. 332, 32-44.

Beinlich, A., Austrheim, H., Glodny, J., Erambert, M., Andersen, T.B., 2010. CO_2 sequestration and extreme Mg depletion in serpentinized peridotite clasts from the Devonian Solund basin, SW-Norway. Geochim. Cosmochim. Acta 74, 6935-6964.

Beinlich, A., Plümper, O., Hövelmann, J., Austrheim, H., Jamtveit, B., 2012. Massive serpentinite carbonation at Linnajavri, N-Norway. Terra Nova 24, 446-455.

Cundall, P. A., and Strack, O. D. L., 1979. A discrete numerical model for granular assemblies, Geotechnique 29, 47–65.

Dash, J. G., Fu, H. and Wettlaufer, J. S., 1995. The premelting of ice and its environmental consequences. Rep. Prog. Phys. 58, 115–167.

Dublet, G., Juillot, F., Morin, G., Fritsch, E., Fandeur, D., Ona-Nguema, G., Brown, G.E., 2012. Ni speciation in a New Caledonian lateritic regolith: A quantitative X-ray absorption spectroscopy investigation. Geochim. Cosmochim. Acta 95, 119-133.

Garnier, J., Quantin, C., Guimaraes, E.M., Vantelon, D., Montarges-Pelletier, E., Becquer, T., 2013. Cr(VI) genesis and dynamics in Ferralsols developed from ultramafic rocks: The case of Niquelandia, Brazil. Geoderma 193, 256-264.

Girard, L., Gruber, S., Weber, S., and Beutel, J., 2013. Environmental controls of frost cracking revealed through in situ acoustic emission measurements in steep bedrock. Geophys. Res. Lett. 40, 1748–1753.

Golightly, J.P., Arancibia, O.N., 1979. The Chemical Composition and Infrared Spectrum of Nickel- and Iron-Substituted Serpentine from a Nickeliferous Laterite Profile, Soroako, Indonesia. Can. Mineral. 17, 719-728.

Holmes, E.P., Wilson, J., Schreier, H., Lavkulich, L.M., 2012. Processes affecting surface and chemical properties of chrysotile: Implications for reclamation of asbestos in the natural environment. Can. J. Soil Sci. 92, 229-242.

Hostetler, P.B., Coleman, R.G., Mumpton, F.A., Evans, B.W., 1966. Brucite in alpine serpentinites. Am. Mineral. 51, 75-98.

Hövelmann, J., Austrheim, H., Beinlich, A., Munz, I.A., 2011. Experimental study of the carbonation of partially serpentinized and weathered peridotites. Geochim. Cosmochim. Acta 75, 6760-6779.

Hövelmann, J., Putnis, C. V., Ruiz-Agudo, E. And Austrheim, H., 2012. Direct nanoscale observations of CO_2 sequestration during brucite [$Mg(OH)_2$] dissolution. Environ. Sci. Technol. 46, 5253–5260.

Kelemen, P.B., Matter, J., 2008. In situ carbonation of peridotite for CO_2 storage. Proc. Nat. Acad. Sci. U.S.A. 105, 17295-17300.

Koch, C.B., 1998. Structures and properties of anionic clay minerals. Hyperfine Interactions 117, 131-157.

Kruissink, E.C. and van Reijen, l.l. 1981. Coprecipated Nickel-Alumina Catalysts for Methanation at High Temperature, J.Chem. Soc. Faraday Trans. 1, 1981, 77, 649-663

Lautridou, J. P., and Ozouf, J. C., 1982, Experimental frost shattering: 15 years of research at the Centre de Gèomorphologie du CNRS. Prog. Phys. Geog. 6, 215–232.

Matsuoka, N., 2008. Frost weathering and rockwall erosion in the southeasternSwiss Alps: Long term (1994–2006) observations. Geomorphology 99, 353–368.

Matsuoka, N., and Murton, J. B., 2008. Frost weathering: Recent advances and future directions. Permafrost Periglac. 19, 195–210.

Miyata, S., 1983. Anion-exchange properties of hydrotalcite-like compounds. Clays Clay Minerals 31, 305-311.

Moore, A.C., Hultin, I., 1980. Petrology, mineralogy, and origin of the Feragen ultramafic body, Sør-Trøndelag, Norway. Norsk Geol. Tidsskr. 60, 235-254.

Navarre-Sitchler, A., Steefel, C. I., Sak, P. B., and Brantley, S. L., 2011. A reactive-transport model for weathering rind formation on basalt. Geochim. Cosmochim. Ac. 75, 7644–7667.

Noiriel, C., Renard, F., Doan, M. L., and Gratier, J. P., 2010. Intense fracturing and fracture sealing induced by mineral growth in porous rocks. Chem. Geol. 269, 197–209.

Oskierski, H.C., Dlugorski, B.Z. and Jacobsen, G. 2013a. Sequestration of atmospheric CO2 in a weathering-derived, serpentine-hosted magnesite deposite: C-14 tracing of carbon sources and age constraints for a refined genetic model. Geochimica et Cosmochimica Acta 122, 226-246

Oskierski, H.C., Dlugorski, B.Z. and Jacobsen, G. 2013b. Sequestration of atmospheric CO2 in crysotile mine tailings of the Woodsreef Asbestos Mine, Australia: Quantitative mineralogy, isotopic fingerprinting and carbonation rates. Chemical Geology, 356, 156-169.

Oze, C., Bird, D.K., Fendorf, S., 2007. Genesis of hexavalent chromium from natural sources in soil and groundwater. Proc. Nat. Acad. Sci. U.S.A. 104, 6544-6549.

Palmer, S.J., frost, R.L. and Nguyen, T. 2009. Hydrotalcites and their role in coordination of anions in Bayer liquors: Anionic binding in layered double hydroxides. Coordination chemistry reviews 253, 250-267.

Pokrovsky, O.S., Schott, J., 2004. Experimental study of brucite dissolution and precipitation in aqueous solutions: Surface speciation and chemical affinity control. Geochim. Cosmochim. Acta 68, 31-45.

Pollard, D. D., and Fletcher, R. C., 2005. Fundamentals of Structural Geology, Cambridge University Press.

Pronost, J., Beaudoin, G., Tremblay, J., Larachi, F., Duchesne, J., Hebert, R., Constantin, M., 2011. Carbon sequestration kinetic and storage capacity of ultramafic mining waste. Environmental Science & Technology 45, 9413-9420.

Rozov, K., Berner, U., Taviot-Gueho, C., Leroux, F., Renaudin, G., Kulik, D., Diamond, L.W., 2010. Synthesis and characterization of the LDH hydrotalcite-pyroaurite solid-solution series. Cement and Concrete Research 40, 1248-1254.

Røyne, A., Jamtveit, B., and Malthe-Sørenssen, A., 2008. Controls on rock weathering rates by reaction-induced hierarchial fracturing. Earth Planet. Sci. Lett. 275, 364–369.

Schwertmann, U., Latham, M., 1986. Properties of iron-oxides in some New Caledonian oxisols. Geoderma 39, 105-123.

Taylor, R.M., Hansen, H.C.B., Stanger, G. and Bender Kocj, C. 1991. On the genesis and composition of natural Pyroaurite. Clay Minerals 26, 297-309.

Thevenot, F., Szymanski, R. and Chaumette, P. 1989. Preparation and characterization of Al-rich Zn-Al Hydrotalcite-like compounds. Clays and Clay minerals 37, 396-402

Tsuji, M., Mao, G., Yoshida, T. and Tamaura, Y. 1993. Hydrotalchites with an extended Al3+ substitution: Synthesi, simultaneous TG-DTA-MS study, and their CO2 adsorbsion behaviors. Journal of Material Research, 8, 1137-1142.

Ulven, O. I., Storheim, H., Austrheim, H., and Malthe-Sørenssen, A., 2014. Fracture Initiation During Volume Increasing Reactions in Rocks and Applications for CO_2 Sequestration. Earth Planet. Sci. Lett. 389C, 132–142.

Van Noort, R, Spiers, C.J., Drury, M.R, and Kandianis, M.T. 2013. Peridotite dissolution and carbonation rates at fracture sufraces under conditions relevant for in situ moneralization of CO_2. Geochimica et Cosmochimica Acta. 106, 1-24.

Walder, J., and Hallet, B., 1985. A theoretical model of the fracture of rock during freezing. Geol. Soc. Am. Bull. 96, 336–346.

Wells, M.A., Ramanaidou, E.R., Verrall, M., Tessarolo, C., 2009. Mineralogy and crystal chemistry of "garnierites" in the Goro lateritic nickel deposit, New Caledonia. Eur. J. Mineral. 21, 467-483.

Wilson, S.A., Dipple, G.M., Power, I.M., Barker, S.L.L., Fallon, S.J., Southam, G., 2011. Subarctic Weathering of Mineral Wastes Provides a Sink for Atmospheric CO_2. Environmental Science & Technology 45, 7727-7736.

Wilson, S.A., Dipple, G.M., Power, I.M., Thom, J.M., Anderson, R.G., Raudsepp, M., Gabites, J.E., Southam, G., 2009. Carbon dioxide fixation within mine wastes of ultramafic-hosted ore deposits: examples from the Clinton Creek and Cassiar chrysotile deposits, Canada. Econ. Geol. 104, 95-112.

Zhao, L., Sang, L.Q., Chen, J., Ji, J.F., Teng, H.H., 2010. Aqueous Carbonation of Natural Brucite: Relevance to CO_2 Sequestration. Environmental Science & Technology 44, 406-411.

Fig. 1

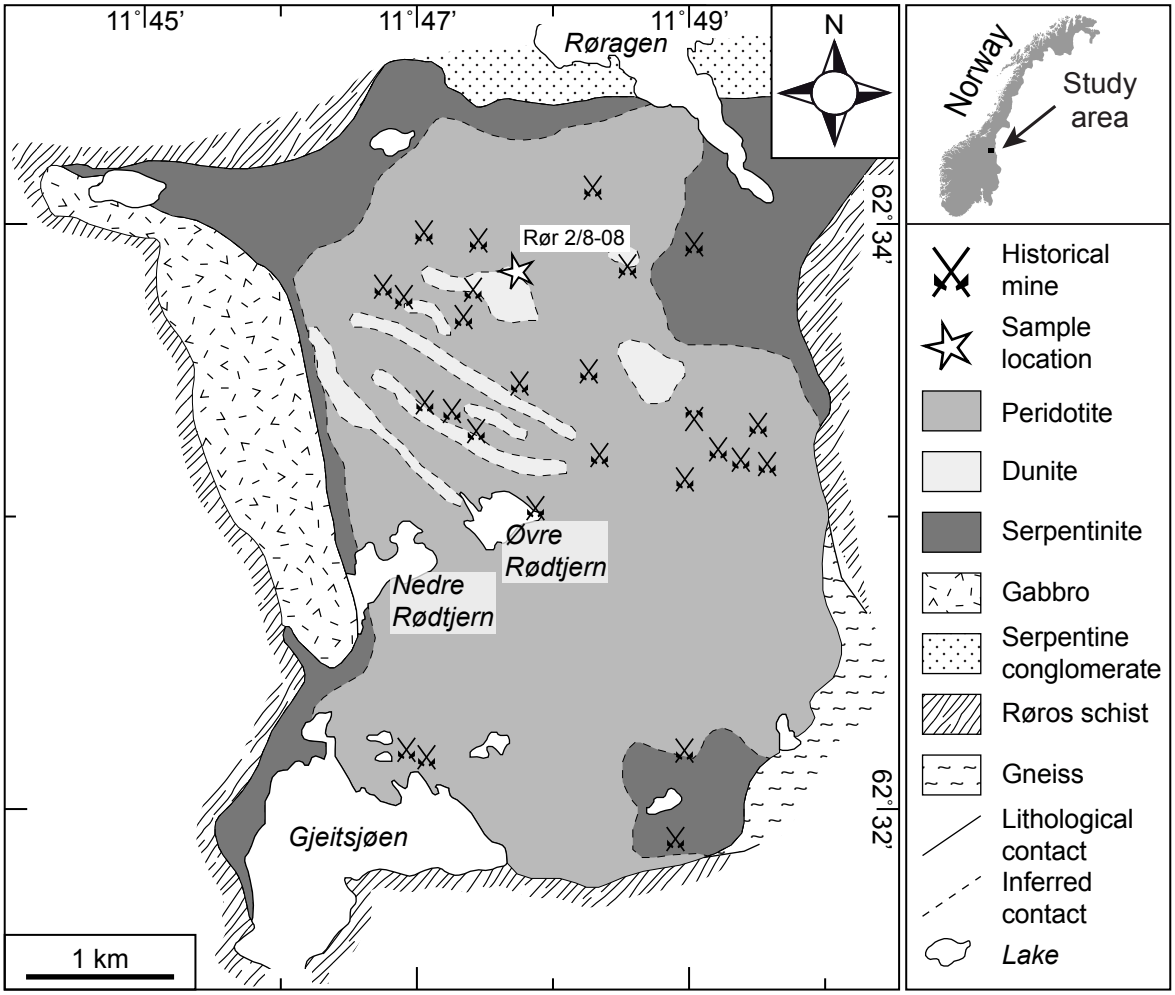
11°45'
11°47'
11°49'
Røragen
N
62°34'
62°32'
Rør 2/8-08
Øvre Rødtjern
Nedre Rødtjern
Gjeitsjøen
1 km
Norway
Study area
Historical mine
Sample location
Peridotite
Dunite
Serpentinite
Gabbro
Serpentine conglomerate
Røros schist
Gneiss
Lithological contact
Inferred contact
Lake

Fig. 2

Fig. 3

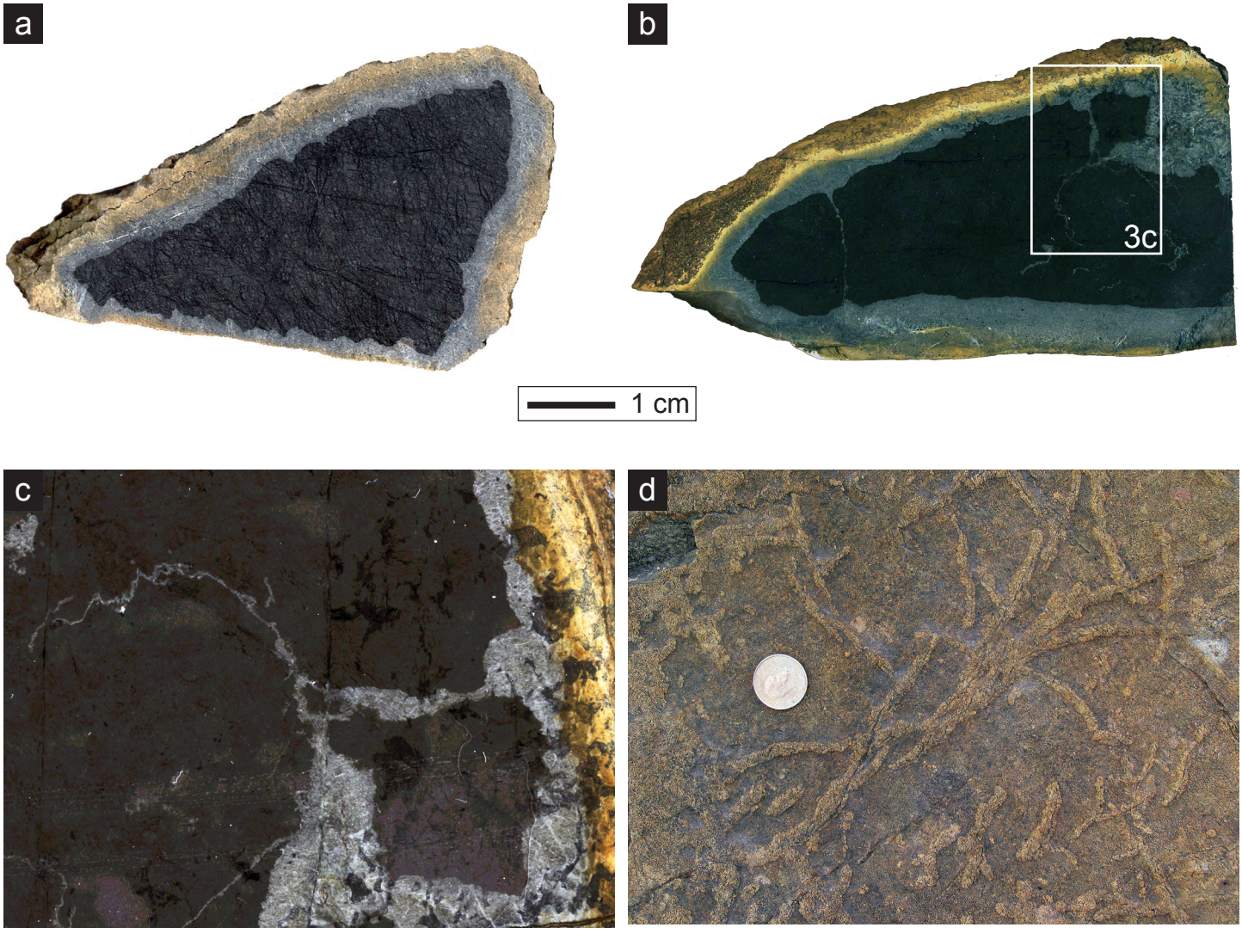

Fig. 4

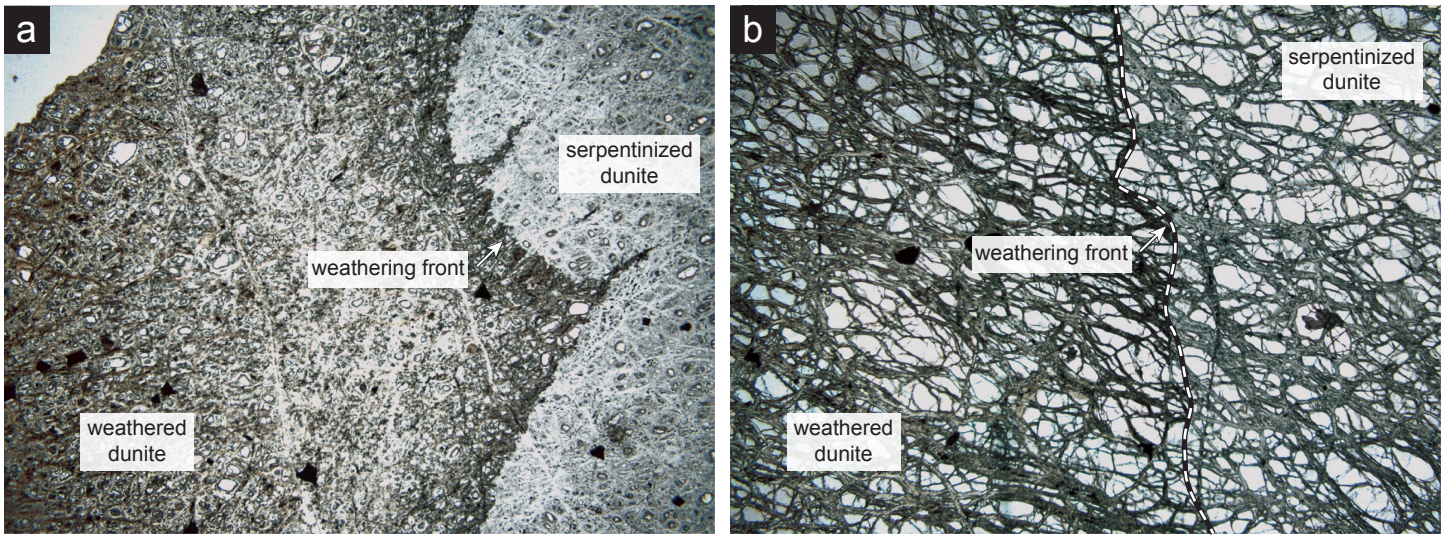
a
serpentinized dunite
weathering front
weathered dunite
b
serpentinized dunite
weathering front
weathered dunite

Fig. 5

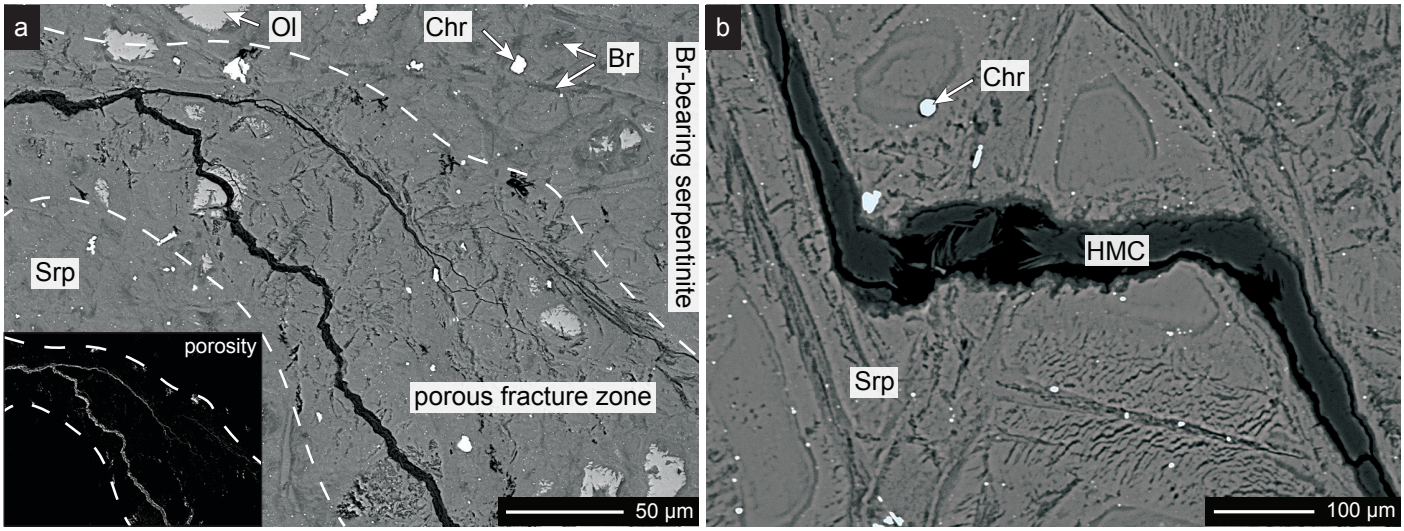
a
Ol
Chr
Br
Br-bearing serpentinite
Srp
porosity
porous fracture zone
50 µm
b
Chr
HMC
Srp
100 µm

Fig. 6

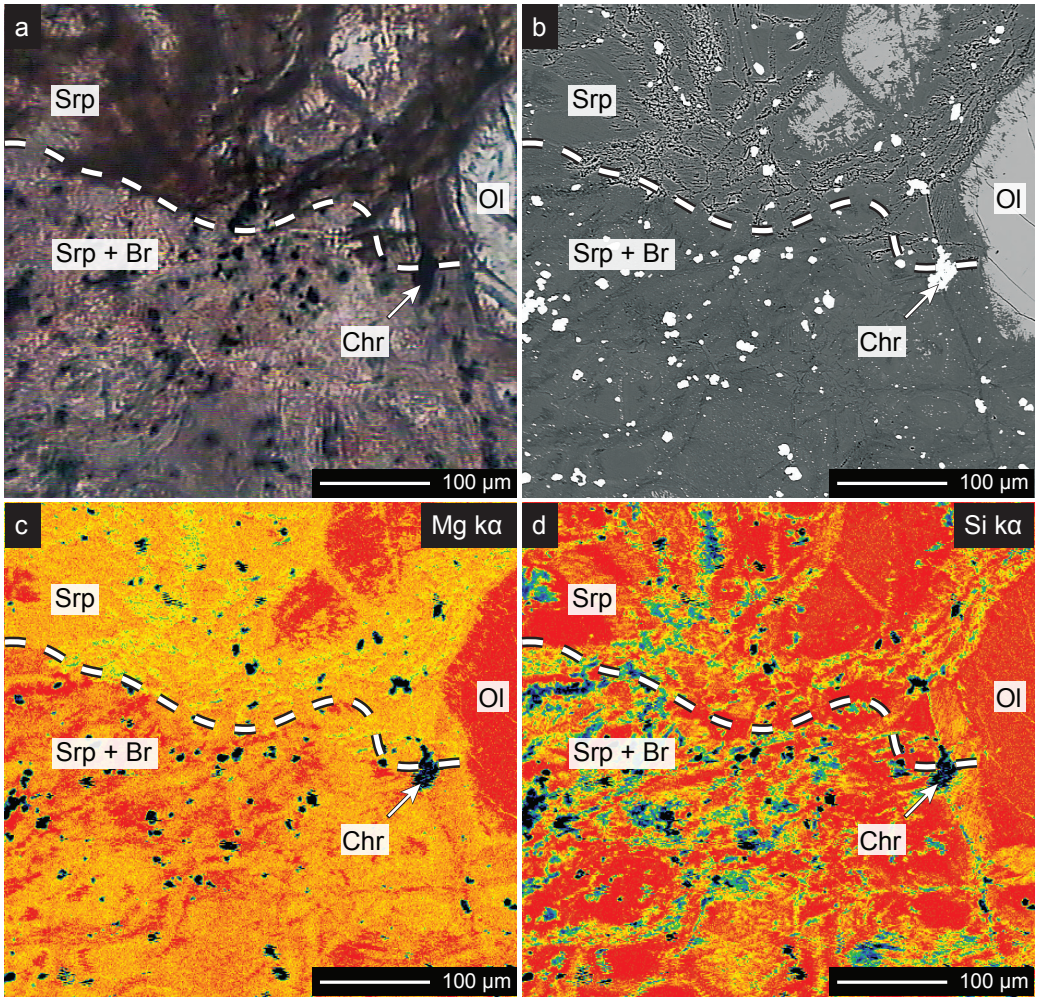
a
Srp
Ol
Srp + Br
Chr
100 µm
b
Srp
Ol
Srp + Br
Chr
100 µm
c
Mg kα
Srp
Ol
Srp + Br
Chr
100 µm
d
Si kα
Srp
Ol
Srp + Br
Chr
100 µm

Fig. 7

Sample: RØR-05-10A

A) Raman maps

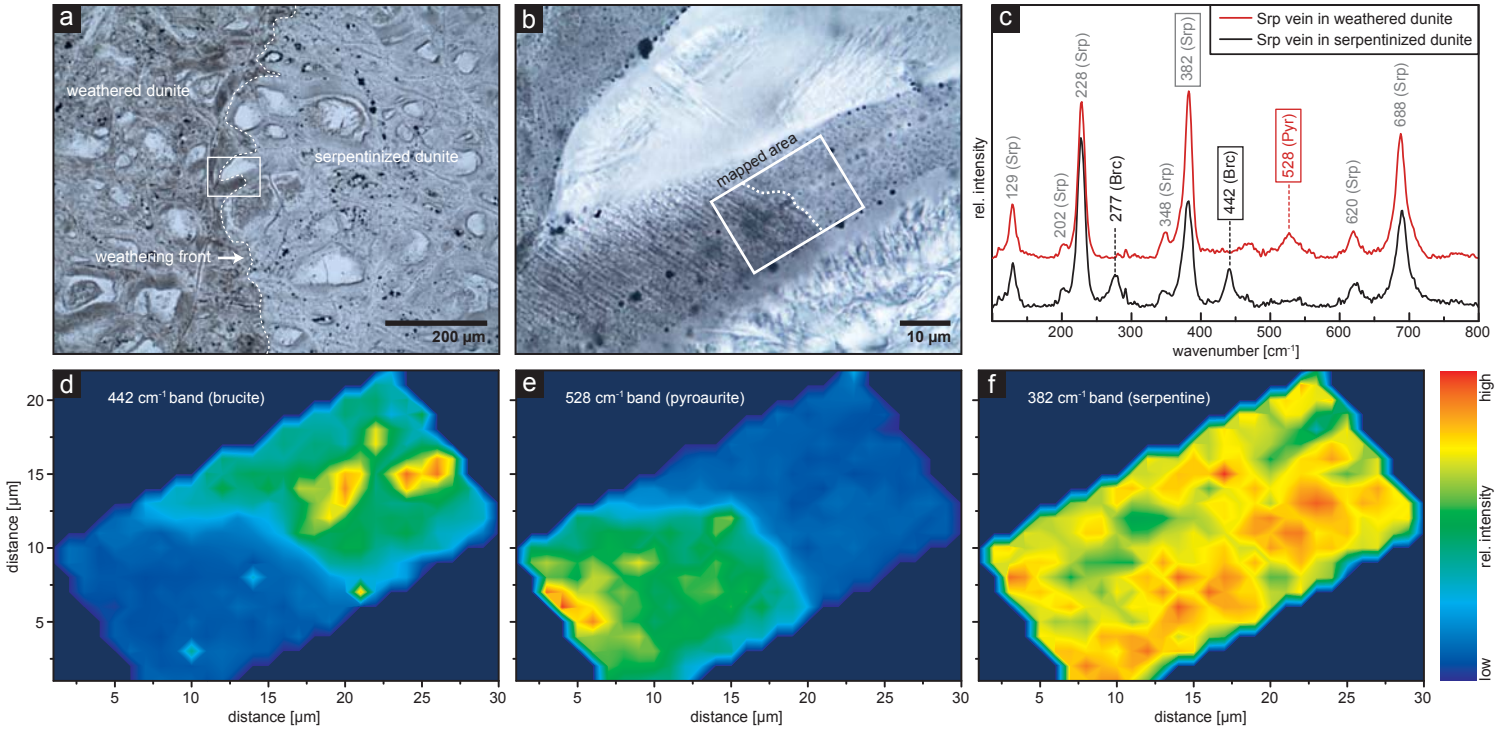

B) Raman line scan

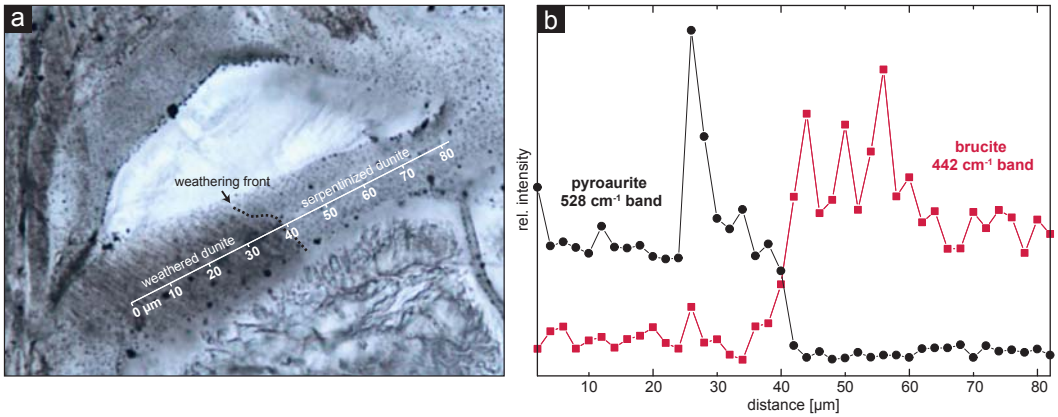

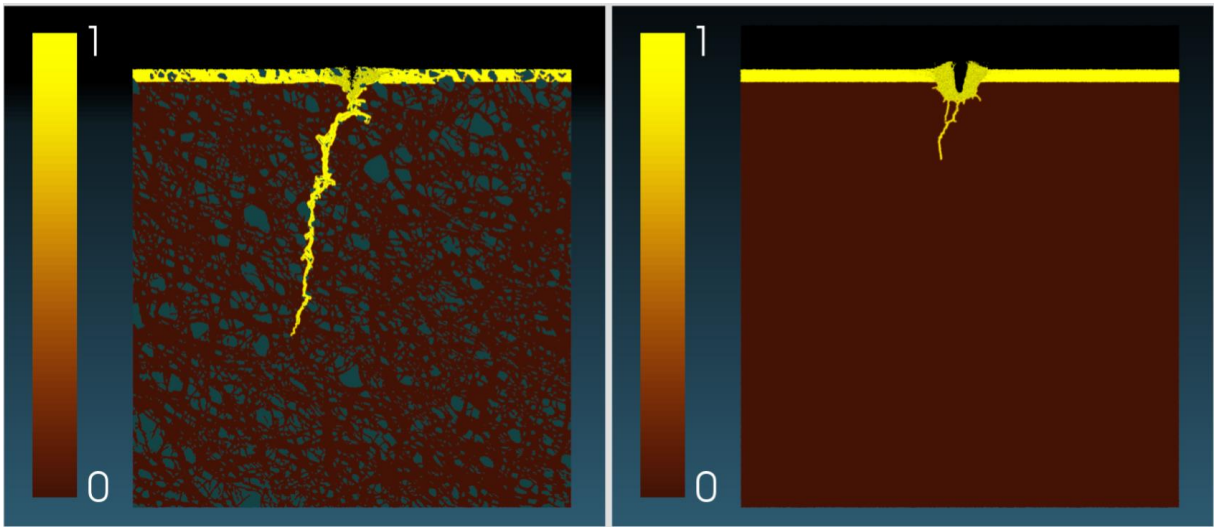
1
0
1
0

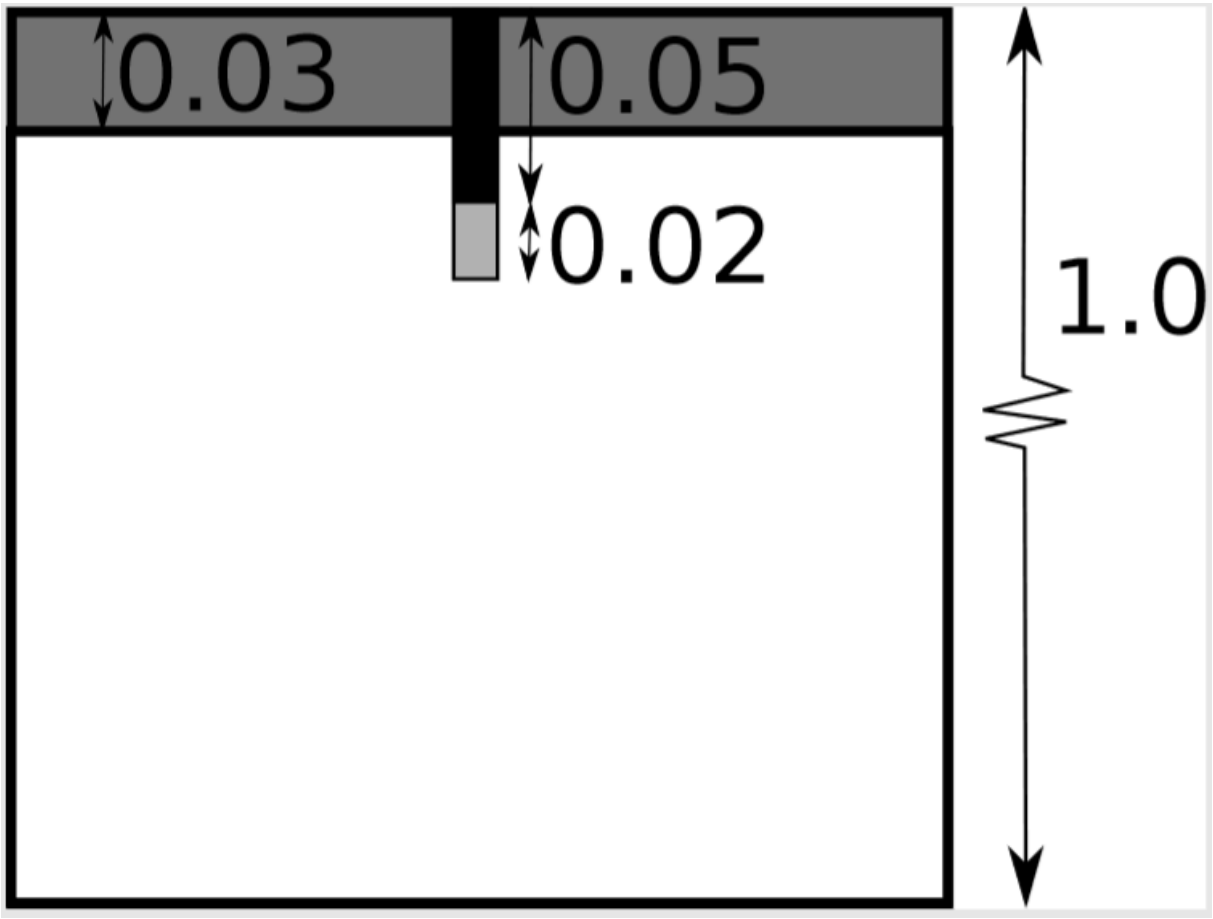
0.03
0.05
0.02
1.0

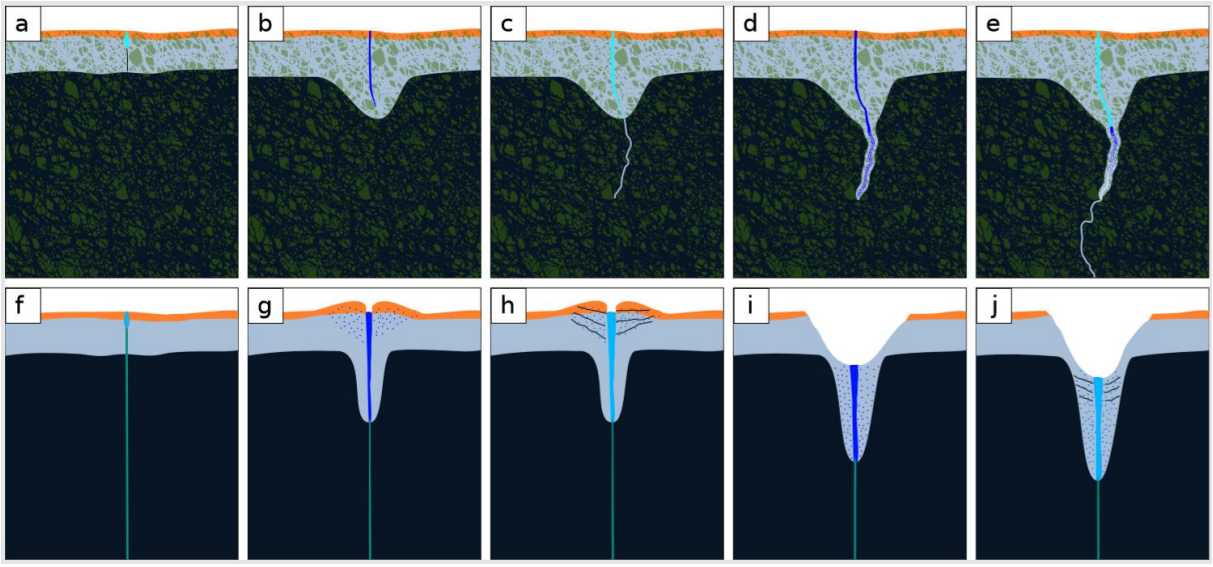
a
b
c
d
e
f
g
h
i
j